Received: 13 July 2022 | Revised: 13 September 2022 | Accepted: 13 September 2022

DOI: 10.1111/jace.18820

Journal of the American Ceramic Society

RESEARCH ARTICLE

The role of Co valence in charge transport in the entropy-stabilized oxide $(Mg_{0.2}Co_{0.2}Ni_{0.2}Cu_{0.2}Zn_{0.2})O$

V. Jacobson[1,2] | **J. Huang**[1,2] | **C.J. Titus**[3] | **R.W. Smaha**[1] | **M. Papac**[5] | **S.J. Lee**[4] | **A. Zakutayev**[1] | **G.L. Brennecka**[2]

[1]National Renewable Energy Laboratory, Golden, Colorado, USA

[2]Colorado School of Mines, Golden, Colorado, USA

[3]National Institute of Standards and Technology, Gaithersburg, Maryland, USA

[4]Stanford Synchrotron Radiation Lightsource, Menlo Park, California, USA

[5]National Institute of Standards and Technology, Boulder, Colorado, USA

Correspondence
G.L. Brennecka, Colorado School of Mines, 1500 Illinois Ave., Golden, CO, USA.
Email: geoff.brennecka@mines.edu

Funding information
National Renewable Energy Laboratory; U.S. Department of Energy, Grant/Award Number: DE-AC36-08GO28308; SLAC National Accelerator Laboratory, Grant/Award Numbers: DOE-SC-BES, DE-AC02-76SF00515; National Science Foundation, Grant/Award Numbers: DMR-1555015, DMREF-1534503

Abstract

Many of the studies on the entropy-stabilized oxide $(Mg_{0.2}Co_{0.2}Ni_{0.2}Cu_{0.2}Zn_{0.2})O$ have been heavily application-based. Previous works have studied effects of cation stoichiometry on the entropy-driven reaction to form a single phase, but a fundamental exploration of the effects of anion stoichiometry and/or redox chemistry on electrical properties is lacking. Using near-edge X-ray absorption fine structure (NEXAFS) and electrical measurements, we show that oxidizing thin film samples of $(Mg_{0.2}Co_{0.2}Ni_{0.2}Cu_{0.2}Zn_{0.2})O$ affects primarily the valence of Co, leaving the other cations in this high-entropy system unchanged. This oxidation increases electrical conduction in these thin films, which occurs via small polaron hopping mediated by the Co valence shift from 2+ to a mixed 2+/3+ state. In parallel, we show that bulk samples sintered in an oxygen-rich atmosphere have a lower activation energy for electrical conduction than those equilibrated in a nitrogen (reducing) atmosphere. Combining feasible defect compensation scenarios with electrical impedance measurements and NEXAFS data, we propose a self-consistent interpretation of Co redox-mediated small polaron conduction as the dominant method of charge transfer in this system.

KEYWORDS
activation energy, charge carrier, entropy, XAS, NEXAFS, XANES, IV

1 | INTRODUCTION

High-entropy oxides (HEOs) have recently gained interest as a class of materials with a variety of tunable properties and many different potential applications. One material in this class is $(Mg_{0.2}Co_{0.2}Ni_{0.2}Cu_{0.2}Zn_{0.2})O$, which has thus far been the only confirmed entropy stabilized material within the HEO family.[1] $(Mg_{0.2}Co_{0.2}Ni_{0.2}Cu_{0.2}Zn_{0.2})O$, commonly known as J14, remains the most studied HEO. J14 is stabilized in a rock salt structure by large configurational entropy due to its five cations. When entropy-stabilized, the cations are homogeneously distributed and have a valence of 2+ in the charge-neutral, stoichiometric system. Each cation species has a different radius and, consequently, the anion sublattice distorts locally to accommodate them.[1]

Prior studies of J14 and its doped derivatives have reported its structure and microstructure, thermal

stability, ionic conductivity, charge compensation mechanisms, magnetic properties, catalytic properties, mechanical properties, and thermal conductivity.[2] However, despite observed redox of some of the transition metal cations in association with lattice distortion and charge redistribution, there are no reports connecting cation valence to electronic transport properties of J14. Cation valence may be affected by synthesis conditions and/or by post-processing conditions that moderate oxygen stoichiometry in the material. Previous studies, including our work, have shown that Co in this system can change valence based on synthesis temperatures, and that electronic conductivity changes dramatically based on growth parameters.[3,4] It has been posited that electronic conductivity is dominated by small polarons[4] in this material. However, a fundamental understanding of the effects of anion chemistry remains lacking. The thermal quenching required to maintain the single phase of J14 has been linked to retained oxygen vacancies in the system.[5]

There are several possible defects that could supply charge carriers in the J14 system. We start by considering oxygen surplus or oxygen deficiency on the system and ignore intrinsic Schottky and Frenkel pairs. We will treat the baseline stoichiometric system as MO, where M represents the collection of nominally-divalent cations (M^{2+}) and O is oxygen (O^{2-}). The transition metal cations also have multiple possible valence states; of particular interest are the oxidation of Co^{2+} to Co^{3+} and the reduction of Cu^{2+} to Cu^{1+}.[6,7] Kröger–Vink notation is used to develop the possible equilibrium reactions in Equations (1)–(6).[8]

Oxygen-excess conditions could be expected to result in either hole-compensated metal vacancies:

$$\frac{1}{2}O_2(g) \leftrightarrow O_O^{\times} + V_M'' + 2h^{\bullet} \quad (1)$$

or in oxidation of cations with compensating metal vacancies:

$$\frac{1}{2}O_2(g) + 2M_M^{\times} + 2O_O^{\times} \leftrightarrow 2M_M^{\bullet} + 3O_O^{\times} + V_M''. \quad (2)$$

Under oxygen-deficient conditions, we would expect to see oxygen vacancies form with the production of free electrons as a means for charge compensation:

$$M_M^{\times} + O_O^{\times} \leftrightarrow M_M^{\times} + V_O^{\bullet\bullet} + 2e' + \frac{1}{2}O_2(g) \quad (3)$$

or for the oxygen vacancy to be charge balanced by reduced cations:

$$2M_M^{\times} + 2O_O^{\times} \leftrightarrow 2M_M' + O_O^{\times} + V_O^{\bullet\bullet} + \frac{1}{2}O_2(g). \quad (4)$$

Finally, cation reduction or oxidation along with the appropriate electronic compensation may happen independently of pO_2 as, respectively:

$$M_M^{\times} + O_O^{\times} \leftrightarrow M_M^{\bullet} + O_O^{\times} + e' \quad (5)$$

or:

$$M_M^{\times} + O_O^{\times} \leftrightarrow M_M' + O_O^{\times} + h^{\bullet} \quad (6)$$

Because these reactions, like the intrinsic Frenkel and Schottky reactions, exhibit no pO_2 dependence, we will lump them into a general background (pO_2-independent) carrier concentration for now; we consider temperature dependence later.

At equilibrium, the rate of reaction is equal for both the forward and reverse reactions. The ratio of the concentrations or pressures of products and reactants is useful for understanding how a reaction may occur. While the actual values of the equilibrium constants themselves are not critical to this report, enforcing global electroneutrality allows us to determine the pO_2 dependence of defect species for each scenario.

In this work, we isolate the role of anion stoichiometry in changes related to cation valence in the J14 system. Previous work has shown electronic conductivity to be higher in thin film samples grown via pulsed laser deposition (PLD) at lower temperatures and pressures (200°C 6.7 Pa (50 mTorr, 0.067 mbar) O_2, denoted as "LTLP") as compared with samples grown at higher temperatures and pressures (450°C 13.2 Pa (100 mTorr, 0.133 mbar) O_2, denoted as "HTHP") with a laser fluence of approximately 1.3 J/cm^2.[4] We determined that the pressure change from 100 mTorr (0.133 mbar) to 50 mTorr (0.067 mbar) was unimportant, though we maintain the naming scheme for consistency with previous work. Lattice distortions were not observed via synchrotron diffraction (Figure S1), suggesting that the changes in electronic conductivity are independent of the Jahn–Teller compression which has been cited in other studies and unlikely to be due to oxygen vacancies.[5,9,10] It should be noted that cation vacancies result in less incremental distortion in the anion-close-packed rock salt structure. This suggests an increase in electronic charge carriers resulting from cation valence shifts, though it has been unclear which cation is primarily affected.[4]

Here, we investigate the effects of synthesis and measurement conditions on electronic conductivity of the ESO $(Mg_{0.2}Co_{0.2}Ni_{0.2}Cu_{0.2}Zn_{0.2})O$ and measure the correlated shifts in cation valence. Previous studies suggested that Cu and Co[3,6,7,11] are the most likely cations to change electronic configuration as a result of changing oxygen content. In addition to the thin film samples, for comparison we synthesized a dense bulk ceramic sample that was also reduced and measured again to clarify the effects of oxygen-deficiency on the system. Linear voltage sweeps (DC) of the thin films at different temperatures reveal electrical activation energy changes as a function of synthesis conditions. A similar set of impedance spectra (AC)

from the bulk sample measured after equilibration in both low pO_2 (a nitrogen environment) and high pO_2 (sintered in flowing O_2, measured in dry air) clarify the role of oxygen stoichiometry in electrical conduction. The correlations between thin film and bulk polycrystalline samples allow for the deconvolution of unknown variables in both sample types. The deposition parameters for thin films do not immediately make it apparent whether samples would be oxygen-rich or oxygen-poor, so the bulk sample analysis allows for clarification on this point. Finally, we report soft X-ray near-edge X-ray absorption fine structures (NEXAFS) data from the J14 thin films and identify which cations are affected by varied oxygen pressure and substrate temperature during synthesis.

2 | EXPERIMENTAL DETAILS

2.1 | Powder preparation

Stoichiometric $(Mg_{0.2}Co_{0.2}Ni_{0.2}Cu_{0.2}Zn_{0.2})O$ powders were synthesized by mixing equimolar amounts of each cation from MgO [Alfa Aesar, 99.99%][1], Co(II,III)O [Alfa Aesar, 99.7%], NiO [Sigma–Aldrich, 99.995%], CuO [Alfa Aesar, 99.995%], and ZnO [Alfa Aesar, 99.99%]. These were roller (ball) milled[12] for at least 6 h in ethanol with yttrium-stabilized zirconia (YSZ) milling media and fish oil as a dispersant. After milling, the powder was calcined in air at 900°C for 8 h and quenched in air. The calcined powder was milled in a planetary mill, using the same parameters, to reduce the particle size. The milled powder suspension was dried overnight to evaporate the ethanol and the dried powder was mixed using a mortar and pestle to negate any flocculation and size segregation during drying. Particle sizes and size distribution were analyzed by a Microtrac S3500 particle size analyzer. The single-phase, calcined powder was then pressed into pellets with a 13 mm diameter under 120 MPa for 3 min. CoO has a tendency to decompose into Co_3O_4 in air, so additional oxygen was added to the sintering atmosphere to prevent this. The pressed green body had a geometric density greater than 50% and was first sintered in a horizontal tube furnace under an oxygen flow with $pO_2 = 83$ kPa (620 Torr). The heating schedule for sintering is as follows: ramp to 750°C at 5°C/min and then to 1100°C at a rate of 10°C/min, followed by an isothermal hold at 1100°C for at least 8 h, then air quench to room temperature.[13]

[1] Certain commercial equipment, instruments, or materials are identified in this paper to foster understanding. Such identification does not imply recommendation or endorsement by the National Institute of Standards and Technology, nor does it imply that the materials or equipment identified are necessarily the best available for the purpose.

The resulting sample was 96% of the theoretical density as measured using a fluid displacement (Archimedes) method. Impedance of this dense sample was measured in flowing air, then the sample was placed back in the tube furnace under a nitrogen flow (pO_2 between 0.5 Pa and 1 Pa) for over 20 h in order to reduce it. This same method (without the N_2 anneal) was used to make a dense $(Mg_{0.2}Co_{0.2}Ni_{0.2}Cu_{0.2}Zn_{0.2})O$ target for thin film growth by PLD, which is detailed below.

2.2 | Pulsed laser deposition

Single-phase films were deposited using a KrF (248 nm) excimer laser with a pulse rate of 20 Hz and laser energy of 200 mJ. Both Zn and Cu from the $(Mg_{0.2}Co_{0.2}Ni_{0.2}Cu_{0.2}Zn_{0.2})O$ target were deposited on the substrate in slightly lower concentrations than the other cations in the target (Zn approximately 1 at% lower, Cu approximately 6 at% lower as measured by X-ray fluorescence). Therefore, CuO and ZnO targets were used to supplement depositions and grow films with equimolar cation concentrations, as confirmed by both X-ray fluorescence and energy dispersive spectroscopy.[4] Substrate temperature and chamber oxygen pressure were used to alter oxygen content in grown films. A substrate temperature of 200°C with 6.7 Pa (50 mTorr, 0.067 mbar) of oxygen was used to grow films designated as "LTLP", while a substrate temperature of 450°C with 13.2 Pa (100 mTorr, 0.133 mbar) of oxygen was used to deposit films designated as "HTHP". Charge transport analysis was done on samples grown on Pilkington NSG TEC 15 Glass with approximately 340 nm of fluorinated tin oxide coating (FTO) with a resistance per square of 13–15 Ω and the NEXAFS portion of the study was conducted on both FTO-coated substrates and borosilicate [Eagle2000] glass (EXG). Within the NEXAFS study, the samples grown on FTO-coated substrates were deposited 4 years prior to the NEXAFS data collection, while the samples grown on EXG substrates were deposited within 1 week of NEXAFS measurements. The older sample set (on FTO-coated substrates) is designated as "aged," while the newer (EXG substrates) samples are referred to as "new." These samples were used to verify stability over time across both HTHP and LTLP sample sets.

2.3 | Electrical measurements

Because the J14 system is metastable and begins to decompose into multiple phases between about 400°C and 875°C, reliable measurements of the single phase could not be collected above 400°C. Both thin film and bulk samples were

measured to clarify oxygen stoichiometry more clearly for each system.

Thin films for electrical characterization were grown on glass substrates coated with FTO, which acted as a continuous bottom electrode. An array of top electrodes was deposited on top of the thin film by electron-beam deposition through a shadow mask in a Temescal FC2000. The top electrodes comprise a 10 nm Ti adhesion layer and 50 nm of Pt. Each circular electrode had a diameter equal to 0.0007 cm^2. Current–density measurements were collected using a Keithley 2400 source meter under electric fields from 0 to ±67,000 V/cm or ±30,000 V/cm. Measurements were taken at discrete points across the entire 5 cm × 5 cm sample using a gold probe with a diameter of 0.4 mm. Measurements were repeated a minimum of 5 times in series to verify repeatability and consistency. Current density was measured at substrate temperatures from 20°C to 142°C. Samples were equilibrated at each temperature for 20 min before the array of points was measured. Thin film experimental data used by this study have been analyzed using the COMBIgor software package[14] and are publicly available in the high-throughput experimental materials database at https://htem.nrel.gov.[15,16] Impedance data and linear voltage sweeps were collected from polycrystalline bulk samples in a vertical tube furnace. Silver electrodes were painted on each side of the sample and cured with Pt wire leads to achieve cohesive electrical contact. The samples were measured using a Gamry Interface 1010E Potentiostat/Galvanostat/ZRA across a frequency range from 10 Hz to 1 MHz. First, the samples were measured while dry air (pO_2 = 17 kPa, 127 Torr) flowed through the tube at temperatures ranging from 350°C down to 150°C in 50°C increments. The sample was equilibrated at each temperature for 30 min before measurement. Next, the sample was removed from the test fixture and annealed at 900°C for over 20 h under a nitrogen flow (pO_2 between 0.5 Pa and 1 Pa, 4 mTorr (0.005 mbar) to 8 mTorr (0.01 mbar) and air quenched. Impedance measurements were repeated in a high-nitrogen atmosphere to evaluate electrical properties of the reduced sample.

2.4 | Near edge X-ray absorption fine structure

NEXAFS measurements of the *L*-edge of Co, Ni, Cu, and Zn and the *K*-edge of O and Mg were carried out on nominally stoichiometric thin films at room temperature at the Stanford Synchrotron Radiation Lightsource (SSRL), SLAC National Accelerator Laboratory, beamline 10-1. Aged HTHP and LTLP films grown on FTO-coated substrates and new HTHP and LTLP films grown on EXG substrates were mounted to an aluminum sample bar using conductive Cu tape. Commercially obtained lithium cobalt(III) oxide (Alfa Aesar, 97%) and cobalt (II,III) oxide (Alfa Aesar, 99.7%) powders were spread directly on electrically conductive carbon tape on the sample bar for reference. The samples were held under high vacuum conditions of approximately 2.7×10^{-6} Pa (2×10^{-8} Torr). A transition edge sensor (TES) spectrometer[17] was used to collect resonant inelastic X-ray scattering (RIXS) planes with a resolution of 2 eV. The energy measured by the TES was calibrated by periodically measuring reference samples of graphite, BN, Fe_2O_3, NiO, and CuO each of which provide a stable set of emission lines. From the RIXS planes, we extracted the L_α and L_β lines to create L-edge partial-fluorescence-yield (PFY) NEXAFS, or the K_α line to create *K*-edge PFY-NEXAFS. Total electron-yield (TEY) NEXAFS spectra were collected by measuring the drain current from the sample. All spectra were normalized by the current measured from a gold grid upstream from the sample.

3 | RESULTS AND DISCUSSION

3.1 | Electronic properties

Current–voltage measurements were conducted on single-phase (Figure S2) thin films grown by PLD on FTO-coated substrates (Figure 1A,B), where those deposited under higher temperature and pressure (HTHP) were significantly less conductive than those deposited under lower temperature and pressure (LTLP) at room temperature. Temperature-dependent resistivity was also measured for each of these samples. An Arrhenius fit of these data shows that the electrical activation energy for HTHP films is approximately 0.5 and 0.3 eV for LTLP films (Figure 1C). An electrical activation energy of 0.3 eV is well correlated with thermally activated small polaron hopping,[18,19] and the 0.5 eV activation energy is likely indicative of small polaron hopping with a higher degree of localization. In Figure 1A,B, the current density measurements do not show a perfectly linear behavior, which is likely the result of imperfect ohmic contact in the electrodes applied for the measurements, or may be related to Joule heating during the measurement. Each fit is a linear approximation of each measurement over the voltage range shown.

The lower activation energy in the LTLP film versus the HTHP film suggests reduced localization for the small polaron hopping in HTHP films, which is in agreement with previous work.[4] Because the temperature and pressure growth parameters have competing effects on oxygen content in thin films, it is difficult to determine exactly

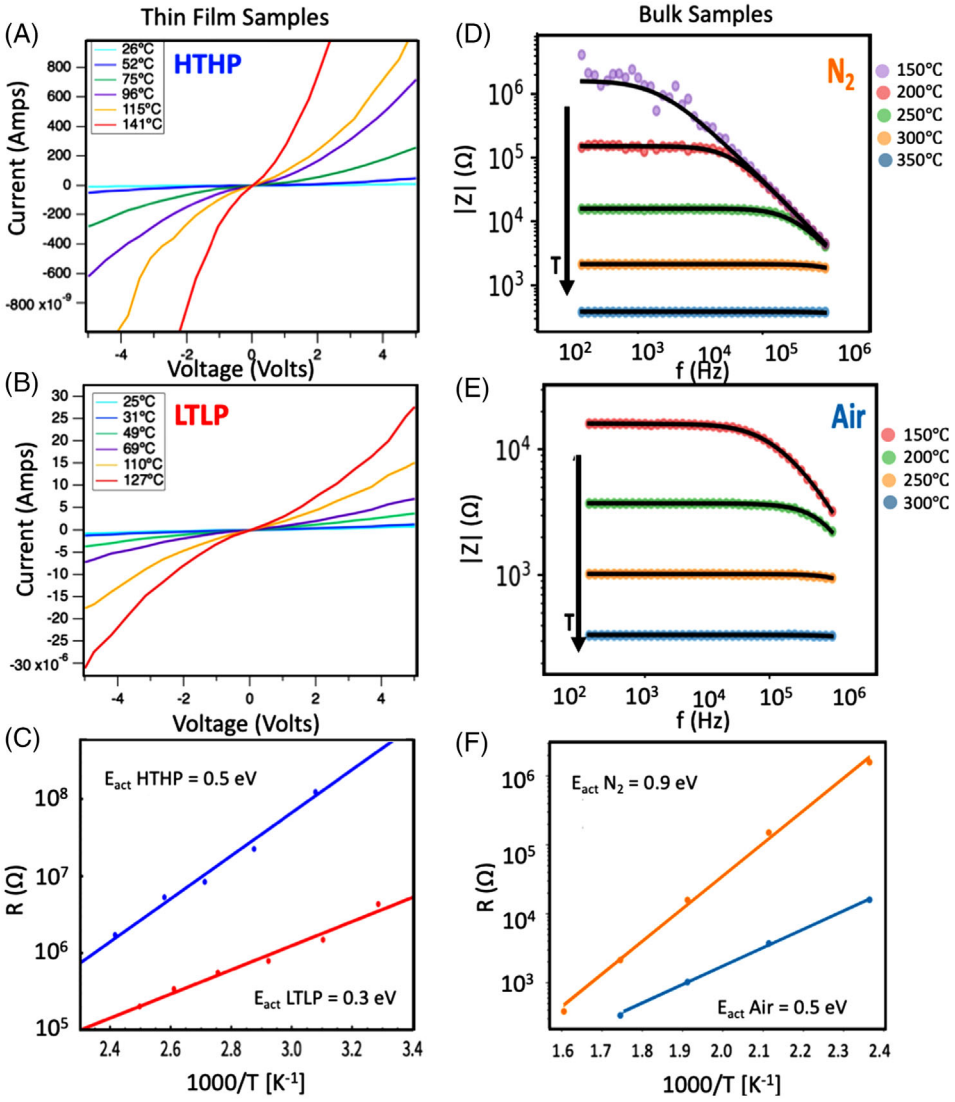

FIGURE 1 Left: IV data in thin films collected on heating for (A) HTHP samples and (B) LTLP samples. (C) The Arrhenius fit of electrical resistance as a function of 1/temperature shows that HTHP films have an activation energy of 0.5 eV and that LTLP films have an activation energy of 0.3 eV. Right: bode plots of the absolute value of resistance for (D) the reduced (N_2) and (E) near-stoichiometric (Air) samples allow for the extraction of total resistance values for each sample at different temperatures. (F) An Arrhenius fit of these data shows that oxygen-poor (N_2) samples have an activation energy of 0.9 eV and near-stoichiometric (Air) bulk samples have an activation energy of 0.5 eV.

how much oxygen is in each sample. Electrical measurements of the bulk sample were used to clarify the role of oxygen in conduction for the J14 family. The bulk sample was initially sintered in flowing oxygen, so it is unlikely to be dominated by oxygen vacancies. After the initial impedance measurements in air were collected, the sample was heated to 900°C and linear voltage sweeps were measured under ultra-high purity (UHP) N_2 flow (pO_2 between 0.5 - 1 Pa, 4 - 8 mTorr, 0.005 - 0.01 mbar) until resistance values stopped changing (approximately 20 h). We took this to be the baseline for nitrogen equilibration in the system. The sample was removed from the system and annealed in a flow of nitrogen for 20 h followed by an air quench, with the expected result being oxygen-deficient single-phase rock salt. Data confirming single-phase rock salt for both of these conditions are in Figure S3. Using these data, we were able to draw parallels between thin film samples (Figure 1A,B) and the bulk results shown in Figure 1D,E.

Arrhenius fits of the data collected in dry air and UHP N_2 (Figure 1F) for the bulk samples show that the activation energy for conduction of the reduced sample (measured in UHP N_2) is approximately 0.9 eV, a value that is often associated with the ionic transport of oxygen vacancies.[20] This is a much higher activation energy than the sample that was sintered in flowing oxygen and

measured in dry air ($E_a \approx 0.5$ eV). We therefore posit that the HTHP film is more oxygen-deficient than the LTLP film because the activation energies follow similar trends and previous studies with annealing support this conclusion.[4] However, these data also indicate that different transport mechanisms occur in thin films from those in bulk samples. From these data, it appears that vacancy-mediated charge transport is the dominant mechanism for oxygen-deficient bulk samples (N_2) and that near-stoichiometric (Air) samples are more likely to be dominated by electron transport, possibly in the form of highly localized small polaron hopping, similar to that of the HTHP samples.[21,22] The LTLP thin film activation energy of 0.3 eV is well correlated with small polaron hopping.[18,19,23] Returning to the defect chemistry addressed in Section 1, the most likely sources of small polarons are either the reduction of Cu^{2+} to Cu^{1+} or the oxidation of Co^{2+} to Co^{3+}. Because we consistently observe higher conductivity—and thus likely higher charge carrier concentrations—for samples processed under higher pO_2 conditions, we propose that the oxidation of Co is a more probable candidate for the increase in electrical conductivity. To investigate this hypothesis, we conducted NEXAFS measurements and analysis on these films.

3.2 | Near edge X-ray absorption fine structures

NEXAFS spectroscopy is a powerful technique for probing the unoccupied electronic states of specific elements. In a NEXAFS measurement, a material is probed with a monochromatic X-ray beam that is swept in energy across an absorption edge, creating core–holes by exciting electrons to unoccupied valence orbitals or bands. The amount of X-ray absorption is measured via the intensity of the electrons or photons that are produced when the core–hole is filled. Changes in the X-ray absorption correspond to the unoccupied density of states, which depends on the oxidation state, spin, and coordination of the elements that are probed.[24] NEXAFS is a unique tool to determine the electronic state of specific elements in both transition metals and light elements such as oxygen.[25,26]

NEXAFS data at the Co, Ni, Cu, and Zn *L*-edges and at the O and Mg *K*-edges for thin film samples were collected using a TES detector[17] for PFY and the drain current from the sample for TEY. As seen in Figure 2, only the Co and O spectra vary between the LTLP and HTHP samples, and all spectra are consistent between aged and new samples. Consequently, we focus on the Co *L*-edge and O *K*-edge more closely to understand how the valence and coordination states of Co may be changing and how those changes alter the available electrical states.

3.2.1 | Co *L*-edge

In the ideal defect-free rock salt J14 system, each cation is divalent, so Co should have a 2+ oxidation state and octahedral coordination. The Co L_3 edge in particular shows prominent peak splitting as a result of electron–electron interactions that promote a multiplet structure, which depends heavily on the coordination of the Co ion in question.[27] Measurements of the Co L_3-edge show that octahedrally coordinated Co^{2+} has a characteristic low-energy peak at 776.5 eV[25] that is not present in either Co^{3+} or tetrahedrally coordinated Co^{2+}. The presence of this shoulder in all scans in Figure 2 in the Co *L*-edge panel in addition to the lack of distortion seen in X-ray diffraction (XRD, Figures S1 and S2) indicates that the rock salt structure is maintained throughout the system, despite any possible change to the valence state. In addition to the low-energy shoulder, in the Co *L*-edge panel of Figure 2, we see a clear, strong Co^{3+} peak at 779.4 eV for samples grown in LTLP conditions, indicating a mixture of Co^{2+} and Co^{3+}. The LTLP spectra can be fit well by a linear combination of the HTHP Co^{2+} spectrum and a reference Co^{3+} spectrum from $LiCoO_2$ (Figure 6) and shows a strong overlay with the Co_3O_4 reference spectrum (Figure 7), which supports the conclusion that the LTLP spectrum is a mix of Co^{2+} and Co^{3+}. The HTHP samples lack a prominent Co^{3+} peak at 779.4 eV, indicating a predominance of Co^{2+} in these samples.

3.2.2 | O *K*-edge

Any incident X-ray with an excitation energy greater than 530 eV can excite an oxygen 1s core electron to an unoccupied state. Each of the five cations in J14 has six oxygen nearest neighbors in an octahedral coordination in the rock salt structure. Understanding the way each of these oxygen nearest neighbors changes the state of local cations can inform our understanding of the local electronic structures and chemical bonds.[26]

When oxygen is bonded to Co^{2+}, the O *K*-edge typically shows a peak split in the 3d orbital range (527–534 eV), which is labeled "Transition metal pre-edge" in Figure 2 in the O *K*-edge panel. In the spectra from the HTHP samples, this peak split is clearly visible, indicating that Co takes on a primarily 2+ valence, though it is likely Co^{3+} has a presence as well. In the spectra from the LTLP samples, there is a much stronger peak around 531 eV, indicating a higher concentration of Co^{3+}, and a small shoulder around 532 eV which may indicate some Co^{2+}. However, these spectra cannot be used to quantitatively compare the concentration of Co in each valence because the peaks and shoulders between 532 and 535 eV are also related to bonding with the

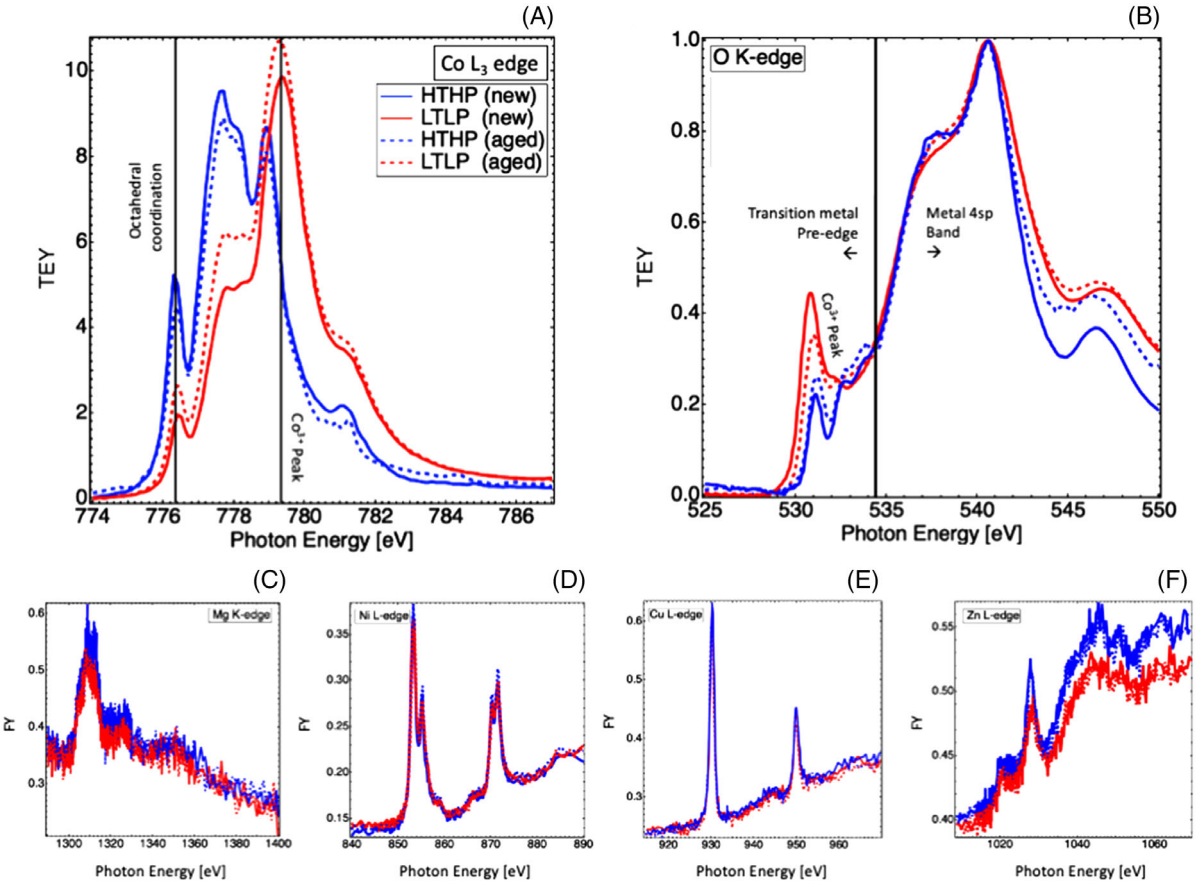

FIGURE 2 Total electron-yield (TEY) and fluorescence-yield (FY) signals are used to show the strongest NEXAFS signals for each element measured. Co and O are the only elements in the J14 composition that change between HTHP and LTLP samples and no noteworthy change occurs with aging. (A) TEY-NEXAFS data collected for Co reveals that the Co charge states and local coordination environments remain constant over time, indicating a higher Co^{3+} content in LTLP samples than HTHP samples. (B) TEY for the O *K*-edge shows that the metal 4*sp* hybridized states remain constant across HTHP and LTLP samples, while the transition metal pre-edge indicates changes in the 3*d* states of the cations. (C–F) Mg, Ni, Cu, and Zn edges all show consistency between HTHP and LTLP samples.

TABLE 1 Property summary

Sample type	Co valence	E_{act} (eV)	Charge carrier	Oxygen content
HTHP thin film	Predominantly 2+	0.5	–	O-deficient
LTLP thin film	2+/3+	0.3	$M_M^{\bullet}$, small polaron	Stoichiometric
Bulk air	(2+/3+)	0.5	–	Stoichiometric
Bulk N_2	(Predominantly 2+)	0.9	Vacancy	O-deficient

Note: Co valence in parentheses is approximated based on trends observed in the present work.

other divalent cations in the system, particularly Ni^{2+}.[26] These data, in conjunction with the Co *L*-edge data from Figure 2 in the Co *L*-edge panel and each of the other near edge spectra, support the hypothesis that Co is the cation responsible for any property changes between films grown as LTLP and those grown as HTHP.

Based on this information, we propose that the oxidation of Co to a valence of 3+ increases conduction across the system and that this conduction is most probably mediated by small polaron hopping.[28–31] This conclusion is also consistent with predictions from the reaction presented in Equation (2).

4 | CONCLUSIONS

The properties summarized in Table 1 suggest that films grown under LTLP are near-stoichiometric, while HTHP

leads to an oxygen deficiency. Over the range studied, partial pressure of oxygen is overshadowed by substrate temperature regarding the incorporation of oxygen into the lattice. Table 1 also shows changes in activation energy and the associated charge carriers for each sample type investigated here. We have also shown that electrical conduction via small polaron hopping is promoted by the oxidation of Co to a 3+ state in thin film samples. Additionally, we have determined that bulk samples have different mechanisms of charge transport than those present in thin films, with the reduced bulk sample showing possible ionic conductivity and the oxidized sample indicating the presence of charge carriers (holes or electrons) for electrical conductivity.

ACKNOWLEDGMENTS

This work was authored in part by the National Renewable Energy Laboratory (NREL), operated by Alliance for Sustainable Energy LLC, for the U.S. Department of Energy (DOE) under contract no. DE-AC36-08GO28308. Work at Mines was supported by the National Science Foundation (DMR-1555015 and DMREF-1534503). Work at NREL was partially supported by the Laboratory Directed Research and Development (LDRD) Program (A.Z.) including Director's Fellowship (R.W.S.). C.J.T. was supported by an NRC Research Associateship award at the National Institute of Standards and Technology. The use of Stanford's Synchrotron Radiation Lightsource, SLAC National Accelerator Laboratory, was supported by DOE-SC-BES under Contract No. DE-AC02-76SF00515. We would like to thank C. Rom for data collection support. The views expressed in the article do not necessarily represent the views of the DOE or the U.S. Government.

ORCID

V. Jacobson https://orcid.org/0000-0002-7704-0882
R.W. Smaha https://orcid.org/0000-0002-8349-2615

REFERENCES

1. Rost CM, Sachet E, Borman T, Moballegh A, Dickey E, Hou D, et al. Entropy-stabilized oxides. Nat Commun. 2015;6:8485.
2. Salian A, Mandal S. Entropy stabilized multicomponent oxides with diverse functionality: a review. CRC Crit Rev Solid State Mater Sci. 2021;0(0):1–52.
3. Kotsonis GN, Meisenheimer PB, Miao L, Roth J, Wang B, Shafer P, et al. Property and cation valence engineering in entropy-stabilized oxide thin films. Phys Rev Mater. 2020;4(10): 100401.
4. Jacobson V, Diercks D, To B, Zakutayev A, Brennecka G. Thin film growth effects on electrical conductivity in entropy stabilized oxides. J Eur Ceram Soc. 2021;41(4):2617–24.
5. Meisenheimer PB, Williams LD, Sung SH, Gim J, Shafer P, Kotsonis GN, et al. Magnetic frustration control through tunable stereochemically driven disorder in entropy-stabilized oxides. Phys Rev Mater. 2019;3(10):1–9.
6. Biesuz M, Spiridigliozzi L, Dell'Agli G, Bortolotti M, Sglavo V. Synthesis and sintering of (Mg, Co, Ni, Cu, Zn)o entropy-stabilized oxides obtained by wet chemical methods. J Mater Sci. 2018;53:8074–85.
7. Diercks DR, Brennecka GL, Gorman BP, Rost CM, Maria J. Nanoscale compositional analysis of a thermally processed entropy-stabilized oxide via correlative tem and apt. Microsc Microanal. 2017;23:1640–1.
8. Smyth D. The defect chemistry of metal oxides. Oxford University Press; 2000.
9. Bhaskar LK, Nallathambi V, Kumar R. Critical role of cationic local stresses on the stabilization of entropy-stabilized transition metal oxides. J Am Ceram Soc. 2020;103(5):3416–24.
10. Rák Z, Maria JP, Brenner DW. Evidence for Jahn–Teller compression in the (Mg Co Ni Cu Zn)O entropy-stabilized oxide: a DFT study. Mater Lett. 2018;217:300–3.
11. Rost C, Rak Z, Brenner D, Maria J. Local structure of the $Mg_xNi_xCo_xCu_xZn_xO$ (x=0.2) entropy-stabilized oxide: an exafs study. J Am Cer Soc. 2017;100(6):2732–8.
12. Rahaman M. Sintering of ceramics. Boca Raton: Taylor & Francis; 2007.
13. Jacobson V, Gann K, Sanders M, Brennecka G. Densification of the entropy stabilized oxide $(Mg_{0.2}Co_{0.2}Ni_{0.2}Cu_{0.2}Zn_{0.2})O$. J Eur Ceram Soc. 2022;42(10):4328–34.
14. Talley K, Bauers S, Melamed C, MCPapac Heinselman K, Khan I, Roberts D, et al. Combigor: data-analysis package for combinatorial materials science. ACS Comb Sci. 2019;21(7):537–47.
15. Zakutayev A, Wunder N, Schwarting M, Perkins JD, White R, Munch K, et al. An open experimental database for exploring inorganic materials. Sci Data. 2018;5:180053.
16. Talley KR, White R, Wunder N, Eash M, Schwarting M, Evenson D, et al. Research data infrastructure for high-throughput experimental materials science. Patterns. 2021;2(12):100373.
17. Lee SJ, Titus CJ, Alonso Mori R, Baker ML, Bennett DA, Cho HM, et al. Soft x-ray spectroscopy with transition-edge sensors at stanford synchrotron radiation lightsource beamline 10-1. Rev Sci Instrum. 2019;90(11):113101.
18. Rettie AJ, Chemelewski WD, Emin D, Mullins CB. Unravelling small-polaron transport in metal oxide photoelectrodes. J Phys Chem Lett. 2016;7(3):471–9.
19. Crevecoeur C, De Wit HJ. Electrical conductivity of Li-doped MnO. J Phys Chem Solids. 1970;31(4):783–91.
20. Hur J. The origin of the exceptionally low activation energy of oxygen vacancy in tantalum pentoxide based resistive memory. Sci Rep. 2019;9:17019.
21. Catlow CR, Corish J, Diller KM, JacobsS PW, Norgett MJ. A theoretical study of intrinsic and extrinsic defect properties of alkali halides. J Phys Colloq. 1976;37(C7):C7-253–C7-259.
22. Walz F. The Verwey transition—a topical review. J Phys Condensed Matter. 2002;14(12):R285.
23. Anirban S, Dutta A. Structure, small polaron hopping conduction and relaxor behavior of Gd_2NiMnO_6 double perovskite. J Phys Chem Solids. 2021;159:110292.
24. de Groot FMF, Kotani A. Core level spectroscopy. CRC Press; 2008.

25. Hibberd AM, Doan HQ, Glass EN, De Groot FM, Hill CL, Cuk T. Co polyoxometalates and a Co_3O_4 thin film investigated by L-edge X-ray absorption spectroscopy. J Phys Chem C. 2015;119(8):4173–9.
26. Frati F, Hunault MO, De Groot FM. Oxygen K-edge X-ray absorption spectra. Chem Rev 2020;120(9):4056–110.
27. Henderson GS, Groot FMFD, Moulton BJA. X-ray Absorption Near-Edge Structure (XANES) spectroscopy. Rev Mineral Geochem. 2014;78:75–138.
28. Ke Q, Lou X, Wang Y, Wang J. Oxygen-vacancy-related relaxation and scaling behaviors of $Bi_{0.9}La_{0.1}Fe_{0.98}Mg_{0.02}O_3$ ferroelectric thin films. Phys Rev B: Condens Matter Mater Phys. 2010;82(2):1–7.
29. Wang XP, Fang QF. Mechanical and dielectric relaxation studies on the mechanism of oxygen ion diffusion in (formula presented). Phys Rev B: Condens Matter Mater Phys. 2002;65(6):1–6.
30. Wang CC, Lei CM, Wang GJ, Sun XH, Li T, Huang SG, et al. Oxygen-vacancy-related dielectric relaxations in $SrTiO_3$ at high temperatures. J Appl Phys. 2013;113(9):1–10.
31. Niobium doping and dielectric anomalies in bismuth titanate. J Am Ceram Soc. 2000;83(3):528–32. https://doi.org/10.1111/j.1151-2916.2000.tb01229.x

SUPPORTING INFORMATION

Additional supporting information can be found online in the Supporting Information section at the end of this article.

How to cite this article: Jacobson V, Huang J, Titus CJ, Smaha RW, Papac M, Lee SJ, et al. The role of Co valence in charge transport in the entropy-stabilized oxide $(Mg_{0.2}Co_{0.2}Ni_{0.2}Cu_{0.2}Zn_{0.2})O$. J Am Ceram Soc. 2023;106:1531–1539.
https://doi.org/10.1111/jace.18820